

Electron spin interferometry using a semiconductor ring structure

Y. K. Kato, R. C. Myers, A. C. Gossard, and D. D. Awschalom

*Center for Spintronics and Quantum Computation,
University of California, Santa Barbara, CA 93106*

(Dated: February 2, 2008)

A ring structure fabricated from GaAs is used to achieve interference of the net spin polarization of conduction band electrons. Optically polarized spins are split into two packets by passing through two arms of the ring in the diffusive transport regime. Optical pumping with circularly polarized light on one arm establishes dynamic nuclear polarization which acts as a local effective magnetic field on electron spins due to the hyperfine interaction. This local field causes one spin packet to precess faster than the other, thereby controlling the spin interference when the two packets are combined.

PACS numbers: 85.75.-d, 78.47.+p

Recent progress in electron spin manipulation using non-magnetic semiconductors includes the ultrafast all-optical scheme¹, electrical control using g-factor engineering in parabolic^{2,3} and coupled quantum wells⁴, the strain induced spin-orbit interaction^{5,6}, and the spin Hall effect⁷, demonstrating the broad scope of techniques that can be achieved using state-of-the-art semiconductor engineering. The flexibility offered by semiconductor spintronics^{8,9,10} is anticipated to lead to novel devices and may eventually become useful for quantum information processing. Another advantage offered by spin systems in semiconductors is their long coherence times. For example, conduction electron spins in *n*-type GaAs can have a coherence time exceeding 100 ns and can be transported over distances exceeding 100 μm .^{11,12} In contrast, the coherence time of the orbital part of the electron wave function is at most a few picoseconds even in high-mobility two dimensional systems. Here, we demonstrate a device which takes advantage of the long coherence time of the carrier spin system. A ring structure is fabricated from *n*-GaAs in which electron spins are optically initialized, split into two different paths, and recombined on the opposite side. Local nuclear polarization gives rise to an additional spin precession phase in one path, causing constructive and destructive interference between the two spin packets.

On a semi-insulating (001) GaAs substrate, 2 μm of undoped Al_{0.4}Ga_{0.6}As and 2 μm of *n*-GaAs (Si-doped for $n = 3 \times 10^{16} \text{ cm}^{-3}$) are grown by molecular beam epitaxy. The interferometer is fabricated from the *n*-GaAs film, while the AlGaAs film underneath acts as an etch stop layer. The substrate is polished to $\sim 200 \mu\text{m}$ prior to processing, and the ring structure [Fig. 1(a)] is defined by standard photolithography techniques. The mesa is formed by selective spray etching¹³ with a mixture of one part NH₄OH (30%) to 30 parts H₂O₂ (35%), and a second photolithography step is performed to define the contact areas. The metal layers for the contacts are deposited by electron beam evaporation in the following order: Ni (5 nm) / Ge (25 nm) / Au (65 nm) / Ni (20 nm) / Au (200 nm). The sample is annealed at 420 °C for one minute to form ohmic contacts, and a

third photolithography step defines a square window on the back side of the substrate. Selective spray etching is used again to etch the substrate from the back, forming a membrane to allow optical transmission experiments. The device has a two-contact resistance of 6.2 kΩ at a temperature $T = 5 \text{ K}$.

To monitor the electron spin dynamics in the device, we employ time-resolved Faraday rotation^{14,15} in the Voigt geometry with the sample growth axis parallel to the optical axis. A mode-locked titanium sapphire laser produces $\sim 150 \text{ fs}$ pulses at a repetition frequency of 76 MHz and its wavelength is tuned to 818 nm to address the band gap of GaAs. A circularly polarized pump pulse injects spin polarized electrons, and the Faraday rotation of a linearly polarized probe pulse measures the electron spin component along the laser propagation direction at a time delay Δt . The laser beams are focused to a spot size of $\sim 30 \mu\text{m}$, and the average laser powers are 500 μW and 60 μW for the pump beam and the

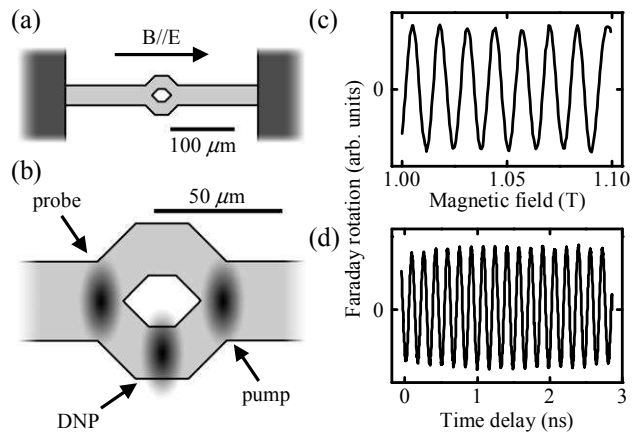


FIG. 1: (a) Device schematic. Dark areas are contacts and light gray area is the GaAs spin interferometer. (b) Schematic of experimental geometry. (c) Faraday rotation as a function of B at $\Delta t = -10 \text{ ps}$ and an applied voltage of 3.5 V. (d) Faraday rotation as a function of Δt at $B = 1 \text{ T}$ and an applied voltage of 3.5 V.

probe beam, respectively. The circular polarization of the pump beam is modulated with a photoelastic modulator at 50 kHz for lock-in detection and Δt is controlled with a mechanical delay line. Measurements are conducted at $T = 5$ K where the longest electron spin lifetimes have been observed.¹¹

We focus the pump beam to the right side of the ring to generate electron spin polarization, while the probe beam detects the spins at the left side of the ring [Fig. 1(b)]. A positive voltage is applied to the contact on the left while the right contact is grounded, establishing an electric field which causes the spins to drift across the structure and into the probe spot. In general, the Faraday rotation signal can be described as

$$\sum_{n=0}^{\infty} S_0 e^{-(\Delta t + nt_{\text{rep}})/\tau} \cos[\omega_L(\Delta t + nt_{\text{rep}})], \quad (1)$$

where S_0 is the amplitude, n is an integer specifying successive pulses, $t_{\text{rep}} = 13.15$ ns is the repetition time of the laser, τ is the spin lifetime, and $\omega_L = g\mu_B B/\hbar$ is the electron Larmor frequency, g is the effective electron g factor, μ_B is the Bohr magneton, B is the applied magnetic field, and \hbar is the Planck constant.¹¹ In order to simplify the data analysis, the voltage is chosen such that only the $n = 1$ pulse contributes to the signal. This is possible as the spin packets from successive pulses are spatially well separated after t_{rep} if a large enough electric field is applied.¹² In Fig. 1 (c), the magnetic field dependence of the Faraday rotation around $B = 1$ T with a bias voltage of 3.5 V is shown. The absence of other harmonic components indicates that pulses with $n > 1$ are not contributing to the signal since the spins generated from earlier pulses have drifted past the probe spot. In Fig. 1 (d), Faraday rotation is plotted as a function of Δt . We see no abrupt jump at $\Delta t = 0$ ns, showing that there is no contribution from the $n = 0$ pulse. This is expected as the pump and the probe spots are spatially separated. The frequency of the spin precession signal is used to extract the electron g-factor, and gives $|g| = 0.42$. We also note that the voltage has been tuned such that the spin precession signal has uniform amplitude throughout the available range of Δt , meaning that the center of the spin packet goes through the center of the probe spot at around $\Delta t = 1.5$ ns. The strain-induced effective magnetic field⁵ plays a negligible role at these large applied magnetic fields.

In order to establish a phase difference between the two paths, optically pumped dynamic nuclear polarization (DNP) is utilized. A circularly polarized third beam with an average power of 5 mW is derived from the same laser and is focused on the lower arm [Fig. 1 (b)]. A slight tilt of the sample causes diffraction of the DNP beam and results in some electron spin polarization along B . A part of the electron spin angular momentum is transferred to nuclear spins, establishing DNP along the applied magnetic field which acts as an additional effective magnetic field for the electron spins through the contact hyperfine interaction.^{16,17} In this manner, the electrons traveling through the lower arm gain an additional phase to their

spin precession. After the two packets have recombined, the expected time-resolved Faraday rotation is

$$A_u \cos(\omega_L \Delta t) + A_l \cos(\omega_L \Delta t + \Phi) = A \cos(\omega_L \Delta t + \phi), \quad (2)$$

where

$$A = (A_u^2 + 2A_u A_l \cos \Phi + A_l^2)^{1/2} \quad (3)$$

and

$$\phi = \tan^{-1} \left[\frac{A_l \sin \Phi}{A_u + A_l \cos \Phi} \right]. \quad (4)$$

Here, A_u and A_l are the amplitudes of the spin packets in the upper and the lower arms, respectively, Φ is the phase difference between the two packets, and lastly, A and ϕ are the amplitude and the phase, respectively, of the combined packet. As Φ is varied, a change in the amplitude of the spin precession signal should occur as a result of the interference term $A_u A_l \cos \Phi$.

We initialize the device by waiting for 30 minutes at $B = 1$ T with the DNP beam on the sample and the bias voltage set to 0 V. The voltage is turned off in an effort to localize the nuclear polarization, while the magnetic field is applied to increase the nuclear polarization.¹⁸ After the nuclear polarization has built up, the DNP beam is blocked, the voltage is set to 3.5 V, and measurements of Faraday rotation as a function of Δt are made repeatedly [Fig. 2 (a)]. Since the DNP beam is turned off, the nuclear spins begin to relax over a timescale of ~ 30 minutes and reduce the phase difference between the two paths. As a consequence, the recombined electron spin polarization at the left side of the ring cycles through constructive and destructive interferences, which manifests as an oscillation in the amplitude of the spin precession signal. Two and a half oscillations are observed in 1500 s, corresponding to a difference in an average effective magnetic field of 28 mT between the two arms.

In order to quantitatively characterize the interference, we fit individual time-resolved Faraday rotation data with $A \cos(\omega_L \Delta t + \phi)$. The parameters A and ϕ obtained from the fits are plotted as a function of lab time in Fig. 2(b) and (d), respectively. The amplitude does not dip down to zero, which is expected if the spin packets from the two arms do not have equal amplitudes. Additionally, the oscillation amplitude increases with lab time, which we attribute to the decrease in signal at early times due to inhomogeneous nuclear polarization that extends to both arms. Diffusion of spin polarized electrons generated by the DNP beam can result in such nuclear polarization, which in turn causes the electron spins used for the interference to dephase. The dephasing will diminish as the nuclear spins depolarize, and this will increase the amplitude of the spin precession signal. This is consistent with the behavior of the phase, which shows an exponential decay with small oscillations superimposed. This decay can be explained by changes in ω_L as a result of nuclear polarization in both arms.

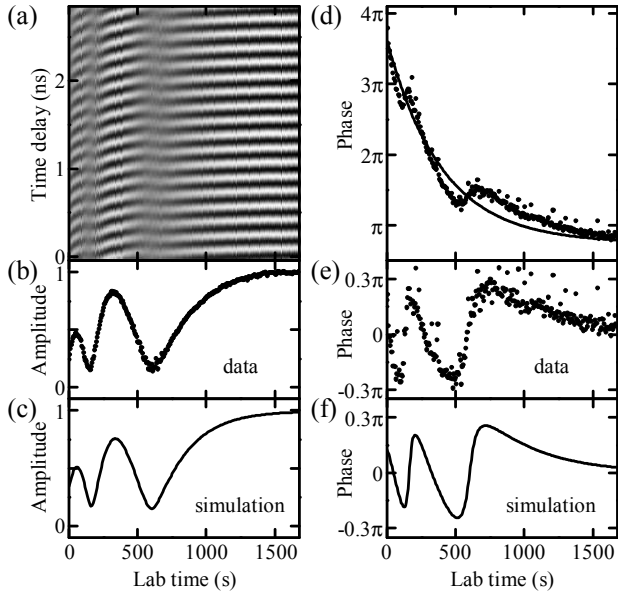


FIG. 2: (a) A series of time-resolved Faraday rotation data as a function of lab time with an applied voltage of 3.5 V at $T = 5$ K and $B = 1$ T. (b) Amplitude of the spin precession signal obtained from fits to data in (a), normalized to the value at $t = 1500$ s. (c) Amplitude of the expected spin precession signal from the simulation. (d) Phase of the spin precession signal from fits to data (filled circles) and exponentially decaying background (line). (e) The data in (d) with the background subtracted. (f) Phase of the expected spin precession signal from the simulation.

Assuming that both the amplitude and the phase difference recover with the nuclear spin relaxation time τ_n , the amplitude of each packet and the phase difference are modeled as

$$A_u = P_u \left(1 - p_u e^{-t/\tau_n}\right), \quad (5)$$

$$A_l = P_l \left(1 - p_l e^{-t/\tau_n}\right), \quad (6)$$

and

$$\Phi = \Phi_0 e^{-t/\tau_n}. \quad (7)$$

Here, P_u and $P_l = 1 - P_u$ are the fractions of upper and lower arms contributing to signal, respectively, p_u and

p_l represent the portions of the signal which have been reduced due to inhomogeneous nuclear polarization, and Φ_0 is the phase difference due to the nuclear polarization between the two paths at time $t = 0$ s. The lab-time dependence of the amplitude and phase of the combined spin packet are simulated from Eq. (3) and (4). The model gives good agreement to data with $P_u = 0.57$, $p_u = 0.45$, $p_l = 0.70$, $\Phi_0 = 4.5\pi$, and $\tau_n = 400$ s [Fig. 2 (c)]. For the analysis of the phase, we have subtracted an exponentially decaying component and an offset given by $\Phi_1 \exp(-t/\tau_n) + 0.75\pi$ with $\Phi_1 = 2.86\pi$ and $\tau_n = 400$ s, which is shown as a solid line in Fig. 2 (d), and the data after subtraction is shown in Fig. 2 (e). The simulation of the lab-time dependence of the phase is obtained from the same set of parameters used in Fig. 2 (c), and is shown in Fig. 2 (f). A good agreement is seen between the data and the model for the phase as well.

The parameters obtained in the analysis allow us to infer the spatial extent of the nuclear spin polarization. Φ_1 gives a measure of the nuclear polarization in the upper arm, while $\Phi_0 + \Phi_1$ gives a measure of that in the lower arm. The ratio of these two values is ~ 2.5 , indicative of significant nuclear polarization in the upper arm. This can be explained by electron spin diffusion, which has been seen to extend to $\sim 15 \mu\text{m}$ in a similar system.¹⁹ In addition, suppression of nuclear spin polarization at the center of a laser spot has also been observed previously,²⁰ and this may be playing a role in keeping this ratio to a relatively small value. There may also be nuclear polarization arising from electron spins excited in the upper arm by tails of the DNP beam.

We note that the interference we observed is of net spin polarization of the electrons, and is not quantum interference^{21,22,23} in the sense that the orbital part of the electron wave function has decohered. We also note that the Aharonov-Bohm effect^{24,25,26} is not expected here as the magnetic field is applied in the plane of the sample.

In summary, we have demonstrated electron spin interferometry using a semiconductor ring structure. It takes advantage of the long lifetime of spin polarization relative to charge coherence, and may find applications in detecting magnetic field gradients. The measurements also provide insights into the effect of nuclear polarization on electron spin dephasing.

We thank G. Salis and acknowledge support from the DARPA and the DMEA.

¹ J. A. Gupta, R. Knobel, N. Samarth, and D. D. Awschalom, Science **292**, 2458 (2001).

² G. Salis, Y. Kato, K. Ensslin, D. C. Driscoll, A. C. Gossard, and D. D. Awschalom, Nature **414**, 619 (2001).

³ Y. Kato, R. C. Myers, D. C. Driscoll, A. C. Gossard, J. Levy and D. D. Awschalom, Science **299**, 1201 (2003).

⁴ M. Poggio, G. M. Steeves, R. C. Myers, N. P. Stern, A. C. Gossard, and D. D. Awschalom, Phys. Rev. B **70**, 121305(R) (2004).

⁵ Y. Kato, R. C. Myers, A. C. Gossard, and D. D. Awschalom, Nature **427**, 50 (2004).

⁶ Y. K. Kato, R. C. Myers, A. C. Gossard, and D. D.

- ⁷ Awschalom, Phys. Rev. Lett. **93**, 176601 (2004).
- ⁷ Y. K. Kato, R. C. Myers, A. C. Gossard, and D. D. Awschalom, Science **306**, 1910 (2004).
- ⁸ S. A. Wolf, D. D. Awschalom, R. A. Buhrman, J. M. Daughton, S. von Molnar, M. L. Roukes, A. Y. Chtchelkina, and D. M. Treger, Science **294**, 1488 (2001).
- ⁹ *Semiconductor Spintronics and Quantum Computation*, edited by D. D. Awschalom, D. Loss, and N. Samarth (Springer-Verlag, Berlin, 2002).
- ¹⁰ I. Zutic, J. Fabian, and S. Das Sarma, Rev. Mod. Phys. **76**, 323 (2004).
- ¹¹ J. M. Kikkawa and D. D. Awschalom, Phys. Rev. Lett. **80**, 4313 (1998).
- ¹² J. M. Kikkawa and D. D. Awschalom, Nature **397**, 139 (1999).
- ¹³ H. Tanobe, F. Koyama, and K. Iga, Jpn. J. Appl. Phys. **31**, 1597 (1992).
- ¹⁴ S. A. Crooker, D. D. Awschalom, and N. Samarth, IEEE J. Select. Topics Quantum Electron. **1**, 1082 (1995).
- ¹⁵ S. A. Crooker, D. D. Awschalom, J. J. Baumberg, F. Flack and N. Samarth, Phys. Rev. B **56**, 7574 (1997).
- ¹⁶ *Optical Orientation*, edited by F. Meier and B. P. Zakharchenya (Elsevier, Amsterdam, 1984).
- ¹⁷ G. Salis, D. D. Awschalom, Y. Ohno, and H. Ohno, Phys. Rev. B **64**, 195304 (2001).
- ¹⁸ J. M. Kikkawa and D. D. Awschalom, Science **287**, 473 (2000).
- ¹⁹ J. Stephens, R. K. Kawakami, J. Berezovsky, M. Hanson, D. P. Shepherd, A. C. Gossard, and D. D. Awschalom, Phys. Rev. B **68**, 41307(R) (2003).
- ²⁰ J. Stephens, J. Berezovsky, R. K. Kawakami, A. C. Gossard, and D. D. Awschalom, Appl. Phys. Lett., **85**, 1184 (2004).
- ²¹ H. A. Engel and D. Loss, Phys. Rev. B **62**, 10238 (2000).
- ²² J. B. Yau, E. P. De Poortere, and M. Shayegan, Phys. Rev. Lett. **88**, 146801 (2002).
- ²³ T. Koga, J. Nitta, and M. van Veenhuizen, Phys. Rev. B **70**, 161302(R) (2004).
- ²⁴ Y. Aharonov and D. Bohm, Phys. Rev. **115**, 485 (1959).
- ²⁵ R. A. Webb, S. Washburn, C. Umbach, and R. A. Laibowitz, Phys. Rev. Lett. **54**, 2996 (1985).
- ²⁶ G. Timp, A. M. Chang, J. E. Cunningham, T. Y. Chang, P. Mankiewich, R. Behringer, and R. E. Howard, Phys. Rev. Lett. **58**, 2814 (1987).